NUMERICAL PREDICTION OF SLAMMING LOADS DURING WATER ENTRY OF BOW-FLARED SECTIONS

(DOI No: 10.3940/rina.ijme.2014.a4.304)

Shan Wang, H B Luo, C Guedes Soares, Centre for Marine Technology and Engineering (CENTEC), Instituto Superior Técnico, Universidade de Lisboa, Lisboa, Portugal

SUMMARY

The two-dimensional water entry of bow-flared sections is studied by using a Multi-Material Arbitrary Lagrangian-Eulerian (MMALE) formulation and a penalty-coupling algorithm. A convergence study is carried out, considering the effects of mesh size, the dimension of fluids domain, and fluid leakage phenomenon through the structure. The predicted results on the wetted surface of a bow-flared section are compared with published experimental values in terms of vertical slamming force, pressure distributions at different time instances and the pressure histories at different points. Comparisons between the numerical results and measured values show satisfactory correlation. An approximation method is adopted to estimate the sectional slamming force and its results are compared with the numerical values, showing good consistency for the peak forces.

NOMENCLATURE

ρ	Density of water (kg m^{-3})
M	Dynamic viscosity
p	Pressure (N m^{-2})
p_0	Pressure of atmosphere (N m^{-2})
g	Acceleration of gravity (m s^{-2})
η	Water surface (m)
F	Total vertical impact force *(N)*
t	Time instance during impact (s)
C_p	Non-dimensional coefficient of p
B	Breadth of the wedge (m)
H	Length of the wedge(m)
V	Vertical impact velocity (m/s)
V_0	Initial impact velocity (m/s)
K	Numerical contact stiffness(GPa)
K	Bulk modulus of the fluid element
p_f	Penalty factor
Y_d	Draft of the body (m)
Y	Vertical coordinates on body surface (m)
Y_k	Vertical coordinate of the keel (m)
H	Submergence of the section (m)
A_{33}	High frequency added mass (kg/m)

1. INTRODUCTION

When a high velocity structure impacts with a nearly incompressible fluid, high peak pressures are created, and its consequences can be hazardous for strength of structures. Ship slamming is a complicated dynamic and fluid-structure interaction problem which is related to many factors, such as relative motion, section shape, characteristics of fluid, hydro-elasticity of structure and others. Slamming is very localised and the duration of the slamming pressure measured at one place on the structure is of the order of milliseconds. For a ship in waves, the position where high slamming pressure occur changes with time. Ship motions and wave induced loads are often calculated by strip theory programs, in which case sectional forces are required and the slamming loads need to be assessed for two dimensional sections corresponding to the ships sections. An example of such an approach is the one adopted by Guedes Soares (1989) who used a method to evaluate the vertical transient load on the ship hull when the forward bottom impacts in water, and later checked it experimentally (Ramos, et al. (2000)). Therefore, reasonable predictions on the pressure distribution on ship sections are necessary and significant.

To predict the pressure distribution during slamming, the idealized problem of a two-dimensional wedge impacting a calm water surface has been initially investigated by von Karman (1929) and Wagner (1932). Since then, Ochi et al. (1973) predicted the slamming characteristics and hull response, and evaluated the non-dimensional factor k for the maximum slamming pressure by a three parameters mapping of a section shape into a circle. Stavovy and Chuang (1976) obtained the k value according to experiments results. Ramos and Guedes Soares (1998) proposed a method to evaluate the vertical transient load by combining the methods of Ochi et al. (1973) and Stavovy and Chuang (1976), and assessed the ship structural response to the vertical slamming induced forces. To assess the slam-induced loads, they considered the ship divided in several transverse strips and looked at each one as a two-dimensional body impacting an undisturbed free surface with a velocity equal to the relative velocity between ship and water. The total load was then obtained by adding the contribution of each strip. The slamming force per unit length of a strip of the ship hull was given by the rate of change of momentum. This is a commonly used approximation method on predicting slamming force, e.g. Fonseca et al. (2006) and Kapsenberg and Thornhill (2010).

By comparing with experimental results from drop tests of ship cross-sections, Zhao and Faltinsen (1993) studied slamming loads on two-dimensional symmetrical sections with and without the effect of flow separation and developed a fully nonlinear solution, and then they

applied the method with good results for a bow flare section. Motivated by the work of Zhao et al. (1996), Mei et al. (1999) raised an analytical solution for the general impact problem by adopting the conformal mapping technique, but their results are valid only for a constant velocity. Yettou (2007) developed this analytical solution to symmetrical water impact problems of a two-dimensional wedge by taking into account the effect of velocity reduction of the solid body upon impact. The two-dimensional water entry of a bow-flared ship section with different roll angle was studied by Sun and Faltinsen (2009) based on a boundary element method, and compared to the tests that were conducted by Aarsnes (1996). By means of experimental measurements, Okada and Sumi (2000) investigated the transitional impact behaviour from a trapped air impact to a Wagner-type impact, and they identified the time histories of the measured pressure as three patterns which were observed at different time instants.

Early research on the numerical simulation of fluid structure interaction can be found in Belytschko (1997) and Zienkiewicz and Bettess (1978). Stenius et al. (2006) considered the water impact of a wedge-shape section by using LS-DYNA. The geometry of the section influences very much the slamming loads, and the selection of the modelling parameters. For example, the numerical fluid leakage was prevented with high contact stiffness in Stenius et al. (2006), however, this solution does not work for the bow-flared section. Alexandru and Brizzolara (2007) predicted the impact loads on both wedge and bow-flared sections using a range of commercial codes (LS-DYNA, SPH, FLOW-3D and FLUENT). Luo et al. (2011) studied the impact loads on a two-dimensional rigid wedge subjected to water entry by using LS-DYNA., Wang et al. (2011) then extends the works to the slamming loads on wedges with different deadrise angles.

This paper presents a further study of the work on numerical prediction of slamming loads for water entry of rigid wedges presented by Luo et al. (2011), Wang and Guedes Soares (2012) and Wang and Guedes Soares (2014), in which good comparison between the numerical predictions and experimental results are obtained. The FE simulation was extended to ship sections with large flare by Wang and Guedes Soares (2013), considering the roll motions. This paper focuses on the selections of the optimum mesh size and dimensions of the fluid domain, aiming at a water-entry simulation for the bow-flared section with high accuracy and low CPU time. The vertical slamming loads, pressure distributions and pressure histories on the wetted surface of a bow-flared section during water entry are predicted. The numerical results are compared with published experimental results. To verify this model, a convergence study for related parameters is carried out. The numerical fluid leakage through the structure is discussed and prevented by using the donor cell advection algorithm. Its effect on the total slamming force is estimated. An approximation method based on momentum theory is studied and used to predict the sectional slamming force on the concerned bow-flared section. The approximated results are compared with the numerical ones.

2. MATHEMATICAL FORMULATIONS

In Arbitrary Lagrangian-Eulerian (ALE) formulations, a reference coordinate which is not the Lagrangian coordinate and Eulerian coordinate is induced. The differential quotient for material with respect to the reference coordinate is described as following equation:

$$\frac{\partial f\left(\vec{X},t\right)}{\partial t}=\frac{\partial f\left(\vec{x},t\right)}{\partial t}+\vec{w}\frac{\partial f\left(\vec{x},t\right)}{\partial x} \tag{1}$$

where, $\vec{X}$ is Lagrangian coordinate, $\vec{x}$ is Eulerian coordinate, and $\vec{w}$ is relative velocity between the particle velocity $\vec{v}$ and the velocity of the reference coordinate $\vec{u}$. Therefore, the ALE formulation can be derived from the relation between the time derivative of material and that of the reference geometry configuration.

Let $\Omega^f \in R^3$ represent the fluid domain, and $\partial\Omega^f$ denote its boundary. The equation of mass, momentum and energy conservation for a Newtonian fluid in ALE formulation in the reference domain, are given by:

$$\frac{\partial\rho}{\partial t}=-\rho div\left(\vec{w}\right)-\vec{w}\cdot grad\left(\rho\right) \tag{2}$$

$$\sigma\frac{\partial\vec{v}}{\partial t}=\vec{div}\left(\overline{\overline{\sigma}}\right)+\vec{f}-\rho\vec{w}\cdot\overline{\overline{grad}}\left(\vec{v}\right) \tag{3}$$

$$\rho\frac{\partial E}{\partial t}=\overline{\overline{\sigma}}:\overline{\overline{grad}}\left(\vec{v}\right)+\vec{f}\cdot\vec{v}-\rho\vec{w}\cdot\vec{grad}\left(E\right) \tag{4}$$

where ρ is the fluid density, f is the body force and σ is the total Cauchy stress given by:

$$\overline{\overline{\sigma}}=-p\cdot\overline{\overline{Id}}+\mu\left(\vec{grad}\left(v\right)+\left(\vec{grad}\left(v\right)\right)^T\right) \tag{5}$$

where p is the pressure and μ is the dynamic viscosity. The part of the boundary at which the velocity is assumed to be specified is denoted by $\partial\Omega_1^f$, the inflow boundary condition is:

$$\vec{v}=\vec{g}\left(t\right)\text{ on }\partial\Omega_1^f \tag{6}$$

The traction boundary condition associated with equation (3) is the condition on stress components. These

conditions are assumed to be imposed on the remaining part of the boundary:

$$\overline{\overline{\sigma}} \cdot \vec{n} = \vec{h}(t) \text{ on } \partial\Omega_h \quad (7)$$

For a single material or multi-material Eulerian formulation, the mesh is fixed in space and materials flow through the mesh using an advection scheme to update fluid velocity and history variables. This takes away all problems associated with distorted mesh that are commonly encountered with a Lagrangian or Arbitrary-Lagrangian-Eulerian (ALE) formulation. Aquelet et al. (2006) concluded that the Euler Lagrange coupling using Eulerian multi-material formulation for the fluid is more suitable for solving slamming problems. The multi-material Eulerian formulation is a specific ALE case where the reference mesh velocity is zero, which means:

$$\vec{u} = 0 \quad (8)$$

Let $\Omega^s \in R^3$, the domain occupied by the structure, and let $\partial\Omega^s$ denote its boundary. A Lagrangian formulation is considered, so the movement of the structure Ω^s described by $x_i(t)(i=1,2,3)$ can be expressed in terms of the reference coordinates $X_\alpha(\alpha=1,2,3)$ and time t

$$x_i = x_i\left(X_\varepsilon, t\right) \quad (9)$$

The momentum equation is given by:

$$\rho\frac{d\vec{v}}{dt} = \overrightarrow{div}\left(\overline{\overline{\sigma}}\right) + \vec{f} \quad (10)$$

where ρ is the fluid density, f is the force density and σ is the total Cauchy stress. The solution of equation (10) satisfies the displacement boundary condition equation (11) on the boundary $\partial\Omega_1^s$ and the traction boundary condition equation (12) in the boundary $\partial\Omega_2^s$.

$$\vec{x}\left(\vec{X}, t\right) = \vec{D}(t) \text{ on } \partial\Omega_1^s \quad (11)$$

$$\overline{\overline{\sigma}} \cdot \vec{n} = \vec{\tau}(t) \quad \text{on } \partial\Omega_2^s \quad (12)$$

where $\vec{n}$ is the unit normal oriented outward at the boundary $\partial\Omega^s$, $\vec{D}(t)$ is the displacement vector and $\vec{\tau}(t)$ is the traction vector.

3. DESCRIPTION OF THE TWO-DIMENSIONAL WATER ENTRY PROBLEM

The Multi-Material Arbitrary Lagrangian-Eulerian (MMALE) outlined in the previous section is validated by experimental data from drop tests for various ship sections with different geometries. Zhao et al. (1996) illustrated the drop tests for a wedge-shape section and a bow-flared section. The sketch of the measured bow-flared section and the location of the pressure sensors (P1-P4) are shown in Figure 1. The pressures on the four points are calculated numerically in this work and compared with the measured values from the pressure sensors. The height of the section *H* is 203*mm*, and the horizontal size *B* is 312*mm*. The mass of the measured section together with the drop rig is 261*kg/m*. The measured section was dropped from a height of 320*mm*, which in return an initial impact velocity $v_0 = \sqrt{2gh} = 2.51m/s$; however, the measured impact velocity was 2.43m/s because of the friction between the test rigs. The time development of the drop velocity in the test was obtained by using the measured vertical velocity in combination with the measured vertical acceleration of the drop rig. Aarsnes (1996) examined the effects of the roll angle on the impact loads and pressures for the bow-flared section with oblique angles though drop tests. For the cases of zero roll angle, two cases of $v_0 = 0.61m/s$ and $v_0 = 2.43m/s$ were tested.

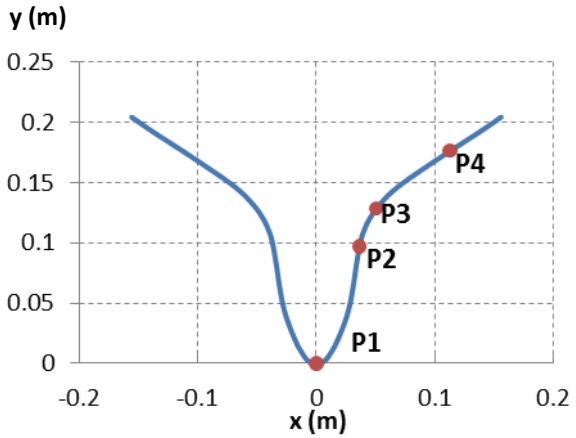

Figure 1. Locations of gauges in bow-flared section (Zhao et al.(1996)).

The explicit finite element method LS-DYNA (Version 971) is applied in this work to simulate the impact between ship section and calm water. Multi-Material Arbitrary Lagrangian-Eulerian (MMALE) formulation and penalty coupling method are applied. The coupling algorithm can be used for problems involving large mesh distortion that cannot be solved by the contact algorithm. However, problems related to numerical fluid leakage through the structure may occur in high velocity impact problems (Aquelet et al. (2006)). Double-precision solver is needed for this simulation, but the double-precision run time will be approximately 30% longer than single-precision run time. Thus, the simulation for water entry of the bow-flared section is more time-consuming than

other explicit analysis. Much effort is needed to decrease the computational time and to obtain accurate predictions. Many researchers proved that mesh size and contact stiffness between Lagrangian and Eulerian elements are of most importance to the numerical results. Besides, a proper time step is required for a stable calculation, and for the advection of the variables at the integration points, an advection scheme is needed to map the state variables of the deformed material configuration back onto the reference mesh. All of these parameters are studied in this work. The numerical model is based on the following main assumptions: the bow-flared section has no deformations; the water is inviscid; the free surface is initially at rest.

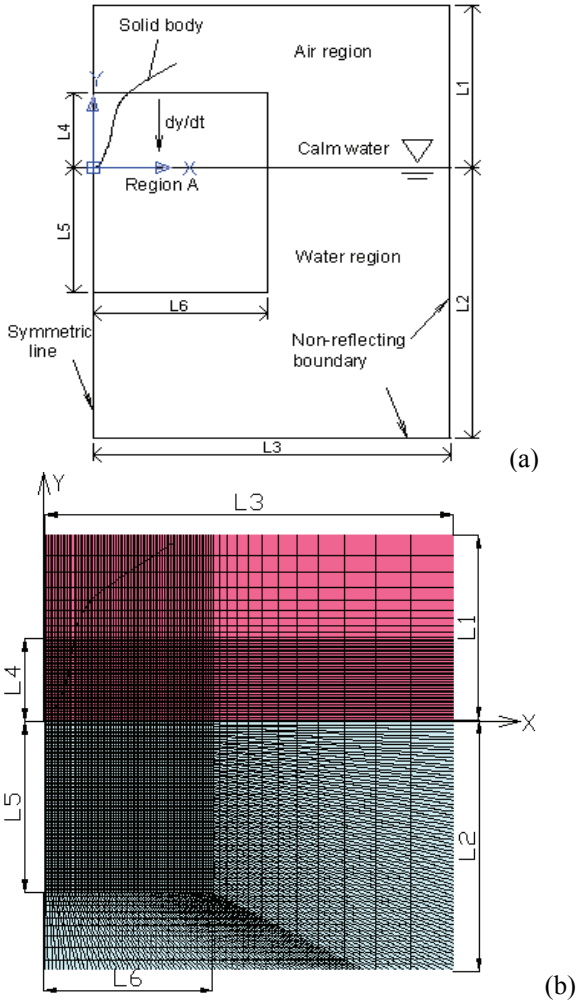

Figure 2. Model setup of the bow-flared section.

The FE model of the water entry problem studied by Zhao et al. (1996) is plotted in Figure 2. As seen in the left figure, only half of the section is modelled. The section drops vertically into the calm water. The *x*-axis is located at the calm water surface, and the *y*-axis is placed in the vertical line which includes the lowest point of the section. The fluid domains consist of air region and water region. Their sizes are illustrated as *L1*L3* and *L2*L3*, respectively. As plotted, the size of the impact domain (region A) are represented as *(L4+L5)*L6*. Symmetric boundary condition is applied in the symmetry line. Correspondingly, the meshed model is shown in the right figure. Region A represents the uniformly meshed area which should satisfy that the finer the mesh of it, the larger size of the area is required. The mesh size and domain size of this region are considered very important to the predictions. Except for this domain, the mesh of other parts is moderately expanded towards the boundaries. Unless otherwise specified, the 'mesh size' in the following means the one of the uniformly meshed area.

The bow-flared section is modelled with shell163 element and rigid body material. The fluid, water and air, are modelled with solid164 element and defined as void materials (*MAT_NULL) (LS-DYNA Keyword User's Manual 2007), which have no yield strength and behave in a fluid-like manner. This material allows equations of state to be considered computing deviatoric stress. Optionally, a viscosity can be defined, however, in this work, the water is considered as inviscid. The state equation of Gruneisen is applied for the water with a density ρ_0=1000kg/m^3 and the bulk sound speed of 1480m/s, and the state equation of linear polynomial is used for the air with the parameters *C4=C5=0.4*. Two-dimensionality is applied by fixing all nodes in the *z*-direction and assuring that the model has only one element in the *z*-direction. The boundaries of the fluids are defined as non-reflecting in order to decrease the effect of the reflection of acoustic wave. Furthermore, pressures are obtained by applying virtual sensors on the center of each shell elements at the coupling surface. Gravity is considered in this work.

4. RESULTS AND DISCUSSION

4.1 MESH DENSITY

Three mesh sizes 5mm, 2.5mm and 2mm are selected for the fluids of the impact domain *(L3*L4*(L5+L6))*. The mesh sizes are denoted by 0.016*B*, 0.008*B* and 0.0064*B*, where *B* means the breadth of the ship section. Unless otherwise specified, the mesh size of the structure is as same as that of the fluids, and the value of P_f is set as 0.1, and the dimension of the fluid domain is *L*1=0.3*m*, *L*2=0.5*m*, *L*3=0.6*m*, *L*4=0.15*m*, *L*5=0.28*m* and *L*6=0.35*m*. In the present work, the numerical contact stiffness k is computed by $k = p_f KA / V$, where K is the bulk modulus of the fluid element in the coupling containing the slave structure node, V means the volume of the fluid element that contains the master fluid node, and A is the average area of the structure elements connected to the structure node. For the three models, the value is *45Gpa/m*, 90 *Gpa/m* and 112.5*Gpa/m*, respectively. The cases with $v_0 = 2.43m/s$ are considered first. Table 1 lists the number of elements (fluid and structure) and CPU time for the three calculations. These results are obtained in the PC with 2GB RAM.

Table 1. The main data for three models with different mesh densities.

Parameters	Model 1	Model 2	Model 3
Mesh size	0.016B	0.008B	0.0064B
Number of elements (Fluids + Structures)	4200+55	13550+110	58560+136
Time step	3.22E-07	1.78E-07	6.04E-08
CPU time	1h 41m	21 h 59 m	89h 43m

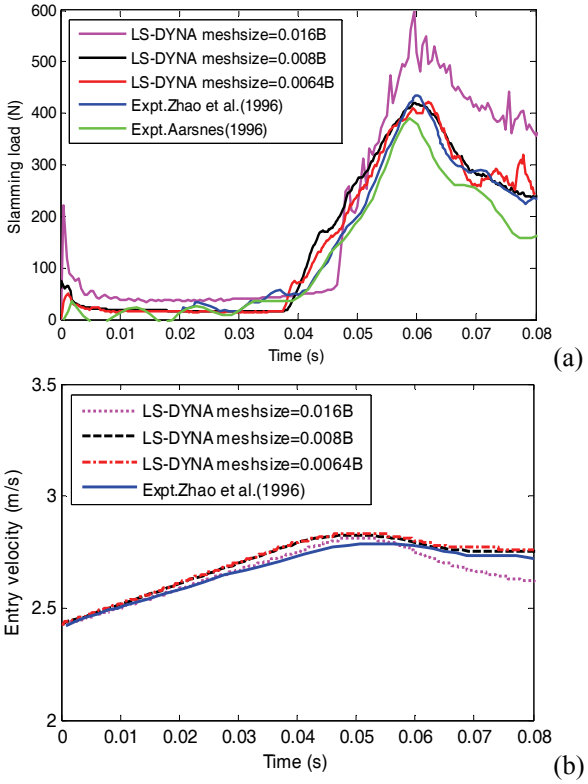

Figure 3. (a) Comparison of the slamming force between numerical and experimental results. (b) Comparison of the entry velocity between the numerical and measured values.

Figure 3 compares the predicted total slamming forces and the entry velocities on the models with different mesh densities, together with the measured values from Zhao et al. (1996) and Aarsnes (1996). As seen in Figure 3(a), some impulses are observed at the first moment when the section touches the calm water, and the value is higher for a coarser mesh density model. At the initial stage, the impact forces are very small for all the curves. This is because the absolute deadrise angle of the lower part of the section is very large, and the added mass on the bow-flared section is small. At the middle stage, the values increase gradually and come to the peak ones around t=0.06*s*, and then they drop fast. When the mesh size is 0.016*B*, the predicted peak force is much higher than the measured values. For the model with coarse mesh density, much numerical noise exists in the results of coupling forces between the slave element and master element, and the impact force is an average value on the section surface, thus an over predicted value is obtained for this model. For the models with mesh densities of 0.008*B* and 0.0064*B*, the predicted peak forces are slightly lower than the experimental value of Zhao et al.(1996), but higher than the one from Aarsnes (1996).

The discrepancies between calculations and experiments are probably due to the three-dimensional and hydroelastic effects in the tests. As seen in Figure 3(b), some differences between the entry velocities are observed in these curves, especially for the late stage of the impact. This is probably one reason for the discrepancies of the impact forces. For the numerical simulations with different mesh densities, the free surface elevations are affected by the mesh size, and then they affect the entry velocities, which cause the discrepancies in the impact forces. The measured entry velocity is lower than the simulated ones, because of the friction effects between the oscillating test rig. When the mesh size is 0.0064*B*, the predicted impact force and entry velocity are in good agreement with the results from the model with 0.008*B*'s mesh size, and some noise exists at the late stage. As listed in Table 1, the CPU time of Model 3 is nearly 5.6 times the one of Model 2, while the predictions of impact force and entry velocity from these two models are similar.

In order to investigate the effects of the discrepancies of the entry velocities on the total slamming load, the measured impact velocity from Zhao et al.(1996) (see Figure 3(b)) is applied to the numerical calculation. The results are compared with the experimental values in Figure 4(a). It shows that the slight difference in the entry velocity does not affect the peak force, but only delays it. The general trends of the curves agree well. Figure 4(b) presents the total slamming forces for the bow-flared section entering water with an initial velocity of -0.61m/s. The results are compared with the calculations from Sun and Faltinsen (2009) by using BEM method and the measured ones from Aarsnes (1996).

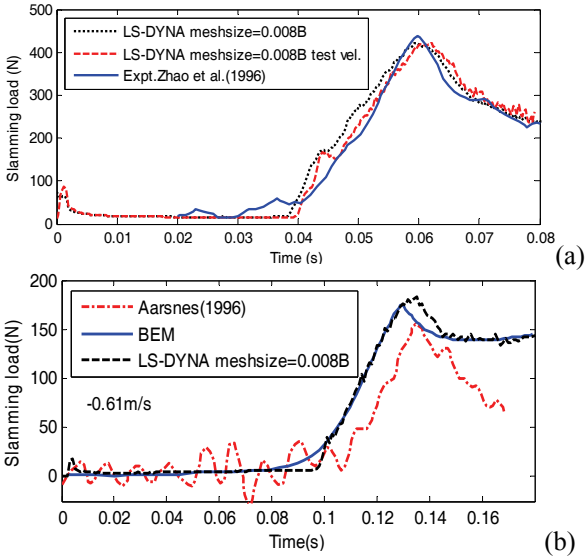

Figure 4. (a) Comparison of slamming loads from the model with drop velocity and the one with the experimental measurement of entry velocity from Zhao et al. (1996). (b) Comparison of the numerical slamming load and the experimental data from the drop test of Aarsnes (1996).

The predictions from LS-DYNA are in good agreement with the BEM's calculations, while the drop tests gave lower measurements. This is consistent with the comparisons of the results for the case with $v_0 = 2.43m/s$. The differences between the tests and the numerical methods are mainly due to the experimental errors which are discussed by Sun and Faltinsen (2008), and other effects caused by three-dimensionalities and hydroelasticity during the tests. Because the same differences are observed for the simulation of 2D wedges in Wang et al. (2012). For a three-dimensional case, the water pileup evolves slower than a two-dimensional case, thus the peak force occurs later. As seen in Figure 3(a) and Figure 4(b), for both cases, LS-DYNA predicts strong oscillations at the late stage. It is because the mesh size of the water jet becomes larger when it goes beyond the impact region. The oscillations seen in the force measurement may due to some vibrations in the test rig.

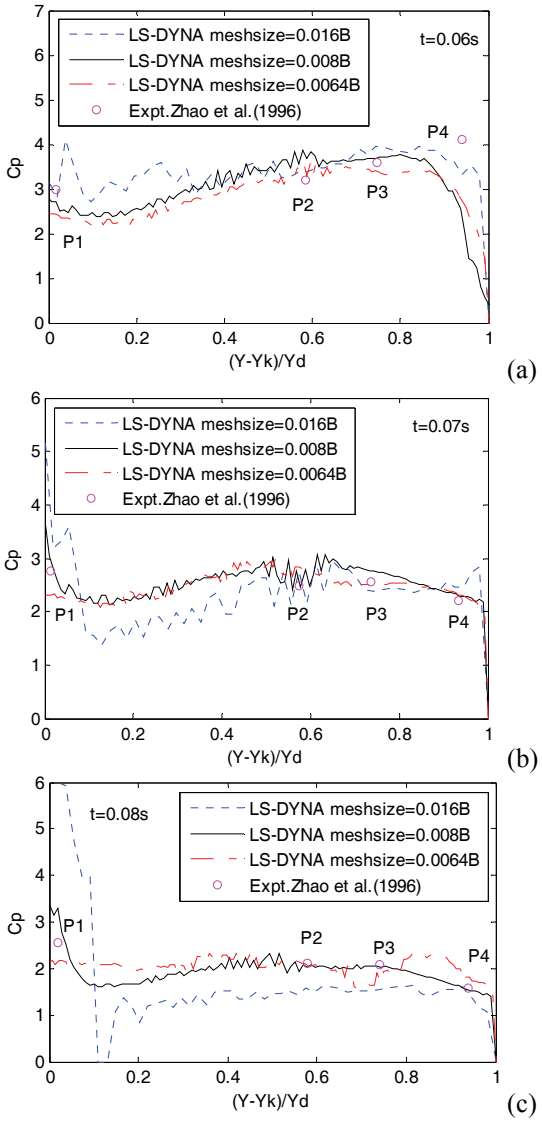

Figure 5. Comparison of the pressure distributions at different moment between numerical and experimental results. (a) t=0.06s, (b) t=0.07s, (c) t=0.08s.

Figure 5 shows the non-dimensional pressure distributions on the wetted surface of the bow-flared section at different time instances, measured values on P1-P4 (see Figure 1) are included as well. For the variables, Y is vertical coordinate on body surface, Y_k is vertical coordinate of the keel and Y_d is the draft of the body, and hence $(Y-Y_k)/Y_d$ represents the position on the body. Pressure coefficient is given by $Cp=P/0.5\rho V^2(t)$, where $V(t)$ is the drop velocity of the body. Pressure distributions for t=0.06s, 0.07s and 0.08s are plotted, where t=0 corresponds to that the keel touches the water surface. The predicted results are in quite good agreement with measured values, especially on the locations of P2 and P3 which are located in the middle part of the section.

When the mesh size is 0.016B, the values of P1 are much larger than the measured values at the time instance of 0.07s and 0.08s. This can be explained as that the mesh size of the vertex of the sections is not finer enough. In the later stage of the water entry, some high numerical noises exist around the vertex of the bow-flared section. When the mesh size is 0.008B, the predicted values have great similarity with the measured ones except that of P1 and P4 at t=0.06s. (see Figure 5 (a)). When the mesh size is 0.0064B, the simulated pressures are somehow smaller than those from the model with 0.008B's mesh size before flow separation. Except that, obvious differences between the results from these two models are found near the keel. When t=0.07s and 0.08s, the measured values of P1 are smaller than the predictions from the model with 0.008B's mesh size, while they are larger than those from the model with 0.0064B mesh size.

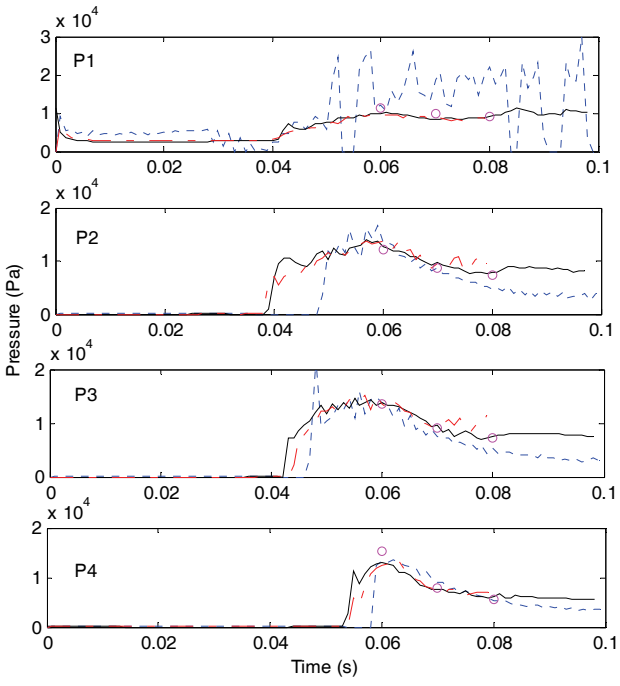

Figure 6. Time histories of the four pressure points on the bottom surface of the section. Dotted line: LS-DYNA with meshsize=0.016B; Solid line: LS-DYNA with meshsize=0.008B; Dash-dotted line: LS-DYNA with meshsize=0.0064B; Round point: Measured values from the drop tests of Zhao et al. (1996).

The predicted time histories of the measured points P1–P4 which are illustrated in Figure 1, are plotted in Figure 6, together with the experimental results recorded at three time moments t=0.06s, t=0.07s and t=0.08s. The predicted values by LS-DYNA agree well with the measured ones on the locations of P2 and P3, but they are usually smaller than the measured ones on the locations of P1 and P4. Since P1 is at the lowest part of the section, the under-estimated values on P1 are due to the mesh size of the model. Corresponding to the vertical force, the predicted peak pressure occurs earlier than the results of the other two methods. When the mesh size is 0.016B, much noise is found on P1 and the rise-up time moments for the four pressure points are delayed due to the water surface elevation. For the models with mesh sizes of 0.008B and 0.0064B, no significant discrepancy is found in the results. In Figure 6, it is observed that about 10*kpa* peak values occur initially on the curves of P1, and they decay very fast. After a period of 0.04s, the second components with a larger duration are observed in the graph. The first component with a large peak and small duration is due to the bottom impact on the water surface, while the second one with larger duration is mainly due to the impact between the large flare and the elevated water.

The corresponding predicted peak values, at the four points are presented in Table 2 which includes the predictions from FLUENT by Alexandru et al. (2007) and the measured ones by the tests of Aarsnes (1996). Compared to the predictions from FLUENT, the results from LS-DYNA are much closer to the measured ones, especially the peak pressure on position P1. Generally, the predictions from LS-DYNA underestimate the peak pressures at position P1, while they overestimate those at positions P2 and P3. The peak pressure on position P4 depends on the mesh size of the model. For the results calculated by LS-DYNA, the values from different models are close, except the ones at P1. It shows that the mesh size has a greater effect on the pressure at the keel. The differences between the numerical results and the measured ones are mainly due to the three-dimensional flow effects of the model tests. The drop tests of Zhao et al. (1996) are carried out for a three-dimensional structure with uniform bow-flared section, while the numerical simulation is performed for a two-dimensional section.

Table 2. Predicted peak pressures from Alexandru et al. (2007)

Point	LS-DYNA (0.008B)	LS-DYNA (0.064B)	FLUENT	Measured pressure
P1(kpa)	25.3	10.1	1302.0	33
P2(kpa)	13.5	15.9	7.0	12.5
P3(kpa)	17.8	15.7	10.6	14.0
P4(kpa)	17.7	14.3	14.7	17.0

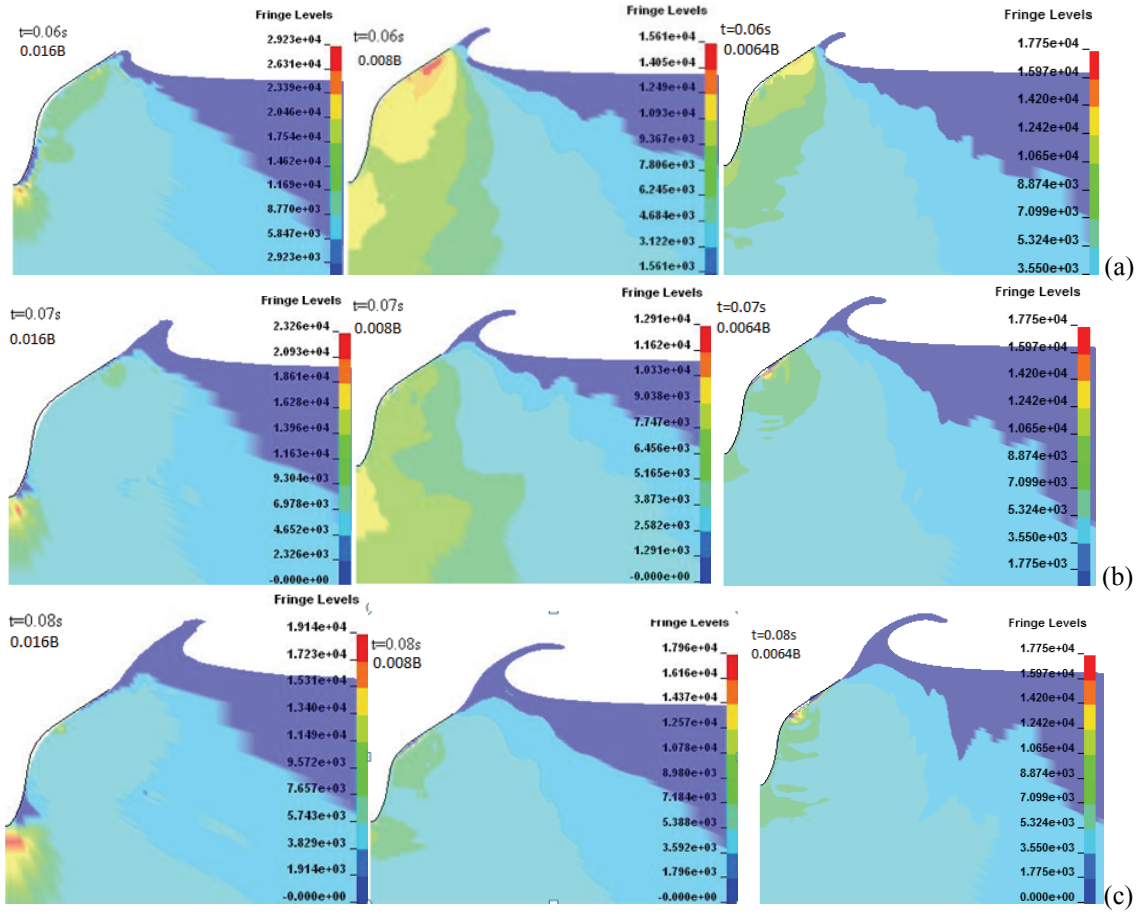

Figure 7. Free surface elevation and pressure contours at different time instances during water entry by LS-DYNA. (a)t= 0.06s; (b) t=0.07s; (c) t=0.08s; t=0 corresponds to that the keel touches the water surface.

Free surface elevation and pressure contours at different time moments for the bow-flared section are shown in Figure 7. These pressure contours present the pressure variations of the entire bow-flared section, which correspond to the pressure distributions plotted in Figure 5. As seen in Figure 4, the total slamming force comes up to the maximum value around t=0.06s, when the peak value of pressure is located near the spray root of the water jet and the section enters under water totally which can be seen in Figure 7(a). After flow separation, the pressure near the spray drops fast, and the peak value moves downwards along the surface of the bow-flared section (see Figure 7 (b)), meanwhile, the pressure of the keel increase gradually. As seen in Figure 7 (c), the peak value of pressure moves to the keel of the section in the later stage of the water entry. When the mesh size is 0.016B, the water surface under the structural bottom evolves relatively slower than other models with finer mesh. This is the reason that the time moment when the impact force begins to increase is delayed to 0.046s for this model as seen in Figure 3(a). When the mesh size is 0.0064B, it seems that the water jet extends to further domain. This may require larger sizes of the impact domain, and thus results in high CPU time.

From the results presented above, it is considered that the models with mesh size of 0.008B and 0.0064B provide satisfactory predictions compared with experimental data. Considering also the CPU time listed in Table 1, it is believed that the model with mesh size 0.008B is an economic and effective option for this work.

4.2 DIMENSIONS OF THE FLUID DOMAIN

To study the effects of the size of fluids domain, five different models are selected. The dimensions of the global fluid domain and Region A are listed in Table 3, where H and B are the height and breadth of the bow-flared section.

Table 3. The main data for the models with different fluid dimension.

Length	Model 1	Model 2	Model 3	Model 4	Model 5
L1/H	1.5	1.5	1.5	1.5	1.5
L2/H	2.46	2.46	2.46	2.46	3.94
L3/0.5B	3.85	3.85	3.85	3.85	7.69
L4/H	0.74	0.74	0.25	0.74	0.74
L5H	1.38	1.38	1.38	0.5	1.38
L6/0.5B	2.25	0.96	2.25	2.25	2.25

Figure 8 presents the predicted total slamming loads from these five models. The results of Model 1, Model 3 and Model 5 are in good agreement with the measured values, while those from Model 4 are much higher. The predictions of Model 3 are in good consistency with the results from Model 1 before t=0.06s, but the results at the late stage are obviously higher. The inconsistency of the predictions from Model 2 is due to water surface elevation at the late stage.

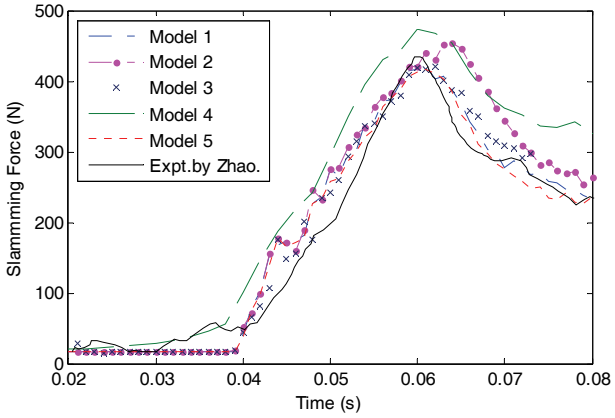

Figure 8. Slamming loads from different models.

As illustrated in Table 3, the size of $L6$ is 0.15m, while the half-width of the section is 0.156m. At the initial stage, the water surface elevation is small, and the mesh size near the impact domain is also small. But at the late stage, the water jet might go far away from the impact domain to the region with coarse mesh.

As seen in Figure 9(a), small water droplets split from the jet due to the coarse mesh in this area. As to Model 4, the size of $L5$ is only 0.1m, and the penetration of the keel into the water is 0.1m around t=0.04s. After the keel of the section goes beyond Region A, lots of high impulse values occur near the keel as seen in Figure 9(b) and (c). Though Model 3 predicts similar results to that from Model 1, the force and pressures obtained from Model 3 are a little larger at the late stage, as plotted in Figure 8. This is also due to the large mesh size of the area that water surface reaches. Since that the predicted force and pressures are very similar for Model 1 and Model 3, considering the computational time, Model 1 is selected in this work.

From the analysis above, it is found that the size of $L4$ and $L6$ affects the numerical results at the late stage, and the size of $L5$ affects the pressure near the keel of section. It can be concluded that the sizes of $L4$ and $L6$ are supposed be as big as the water jet might reach, and the size of $L5$ is supposed to be not smaller than the penetration of the section.

4.3 NUMERICAL FLUID LEAKAGE THROUGH THE STRUCTURE

Fluid leakage is the phenomenon that the fluid penetrates into structure during interacting which can be seen in Figure 10(a). In such a case the fluid particle penetrates through the structure because the coupling force is not large enough to return it to the coupling interface. LS-DYNA Keyword User's Manual (2007) indicates that adjustment can be made on the penalty factor, the number of coupling points, the minimum volume fraction of a fluid to activate coupling and coupling leakage control factor so as to prevent leakage. However, these parameters do not work effectively for the slamming problem in this paper. Much work has been done

on preventing the fluid leakage, but the general solution is still unclear. Low contact stiffness leads to this problem on the simulation of a wedge in Stenius et al. (2006). However, high contact stiffness does not help solving it in this work. It is found that the advection method for the remap step has some effect on this problem. In general, it is recommended to begin an ALE analysis with a Van Leer advection technique. In this paper, the fluid leakage is prevented by using the donor cell advection algorithm (METH=1) (see Figure 10(b)). However, numerical fluid leakage through the structure is a very difficult and complicate problem and depends on the specific situation.

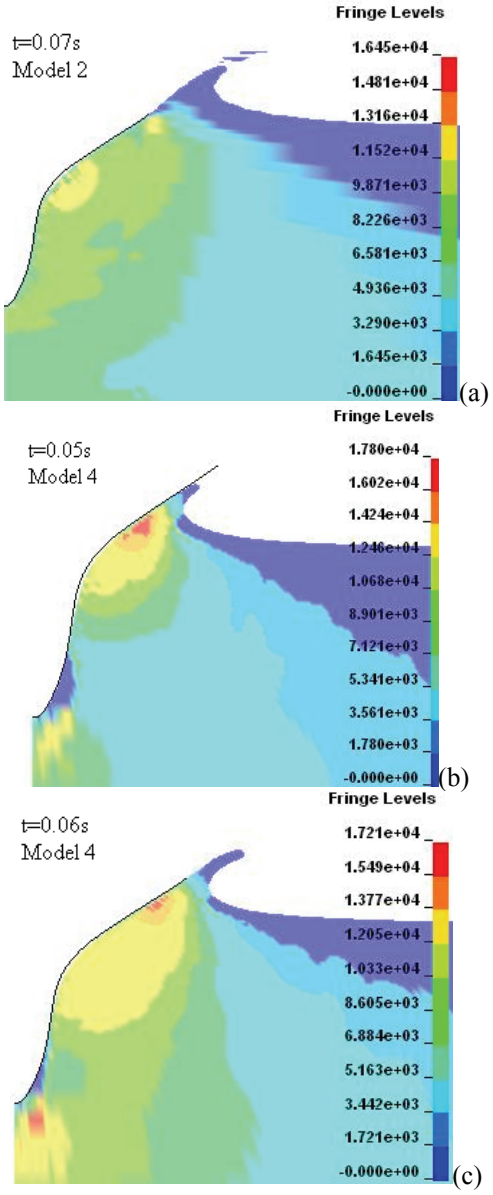

Figure 9. (a) Pressure contour and free surface elevation for Model 2 at t=0.07s. (b) Pressure contour and free surface elevation for Model 4 at t=0.05s. (c) Pressure contour and free surface elevation for Model 4 at t=0.06s.

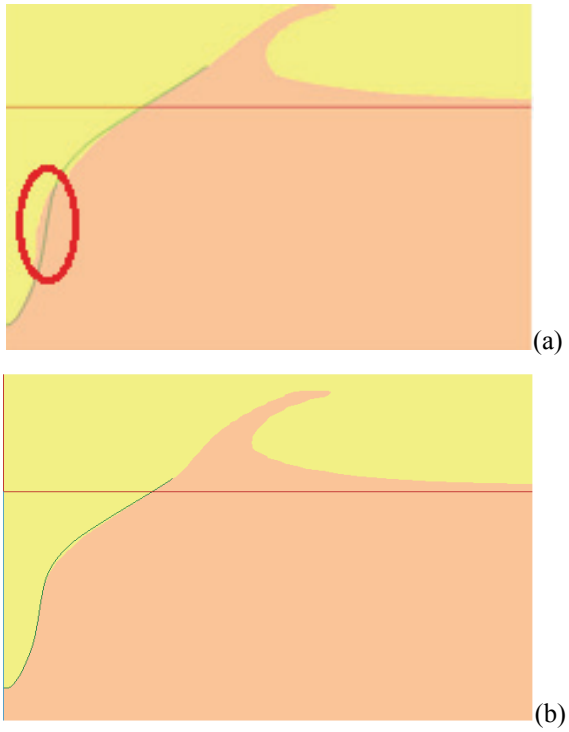

Figure 10. Sketches of fluid leakage through structure during water entry. (a) Fluid leakage; (b) leakage prevented.

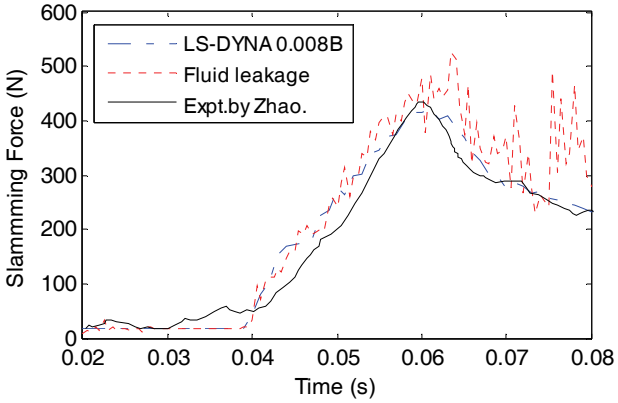

Figure 11. Comparison of the total slamming forces from the cases with and without fluid leakage.

Figure 11 compares the predicted vertical slamming force from the models with and without fluid leakage. The experimental results are included as well. Though the fluid leakage begins at 0.04s after the impact, the results have limited differences before 0.06s. This can be explained because the fluid leakage is not significant at the initial stage. There are much high frequent oscillations in the curve after 0.06s; however, the predicted total slamming forces in the case of fluid leakage are similar to that from the model without leakage at the middle stage. At the later stage, the fluid leakage extends to a large amount, so the slamming force increases due to the large penetration through structure. Therefore, the fluid leakage has a small effect only on the simulated results if it is limited to some extent. Since it

may lead to instability and high frequent oscillation in the simulation, this problem is needed to be prevented.

4.4 APPROXIMATION METHOD BASED ON MOMENTUM THEORY

Guedes Soares (1989) assumed that the slamming force is given by the sum of two components. The first one is an impact component related to the impact of bottom on the water surface and characterized by a large peak with small duration. The second one is given by the rate of change of the hydrodynamic momentum as the hull enters into the water. Flare slamming is accounted by the rate of change of the second component. Following this proposal, Fonseca et al. (2006) made calculations for two different sections, to study the relation between the cross section geometry and the characteristics of the slamming forces. Their results justified that the momentum slamming force is the main part for the section with a large flare, for which the cross sectional slamming force is given by following expression:

$$F_{impact} = \frac{D}{Dt}(A_{33}V) = A_{33}\frac{dV}{dt} + V\frac{dA_{33}}{dt} \qquad (13)$$

where A_{33} is the high-frequency added mass in heave for the body, V is the vertical relative velocity between the cross section and the wave elevation. When the submergence of the body relative to calm water is h, Eq. (13) can be written as:

$$F_{impact} = A_{33}\frac{dV}{dt} + V^2\frac{dA_{33}}{dh} \qquad (14)$$

and for with a constant entry velocity,

$$F_{impact} = \frac{D}{Dt}(A_{33}V) = V^2\frac{dA_{33}}{dh} \qquad (15)$$

The sectional added mass A_{33} is calculated by using the conformal mapping transformation method which was presented by Ramos and Guedes Soares (1997).

For the section plotted in Figure 1, the added masses for different submergence are calculated until the submergence equals to the vertical dimension of the section, as plotted in Figure 12 (a), and the infinite frequency added mass per unit length as a relation between the submergence is shown in Figure 12(b). The results show that the added mass is very small for a low submergence, and the value increases fast after h=0.15, where the flare becomes larger. Two cases are considered here. The first one is the section with a constant velocity V=-2.43m/s, and the second one is the section with an initial velocity V_0=-2.43m/s. The model with 0.008B's mesh size is used for the numerical calculations. According to Eq. (14-15), the estimated slamming forces are calculated until the free surface crosses the static waterlines. The results per unit length are compared in Figure 13, showing that the maximum forces from the derivative of added mass are higher than the numerical ones. This is consistent with the results for the wedges with different deadrise angles shown in Figure 6 of Wang and Guedes Soares (2012).

For the approximate results, there are no initial peaks because the angle of the section is small. The added masses per unit length are calculated with respect to the undisturbed water line, without considering the pile-up effects. The actual water line is significantly higher as seen in Figure 7, and the relative velocity is also higher as the water surface moves up. The section submerges into the water completely around h=0.16m, when the peak forces occur, for the numerical prediction, and then the forces drop fast because the flow separates from the bottom. For the approximate method, the slamming forces are calculated until the sections submerge under the water completely, because the high frequency added masses are calculated until that moment. Without considering the pile-up of water, the sections enters into water totally at h=0.203m which is the vertical dimension of the structure. Kapsenberg and Thornhill (2010) developed a procedure to calculate slamming force based on momentum theory with considering the pile up effects, and they found that good predictions could be found due to a special method to estimate the actual intersection of the free surface. Another disadvantage of this approximate method is the flow separation stage could not be predicted. The increasing process of the slamming force can only be predicted.

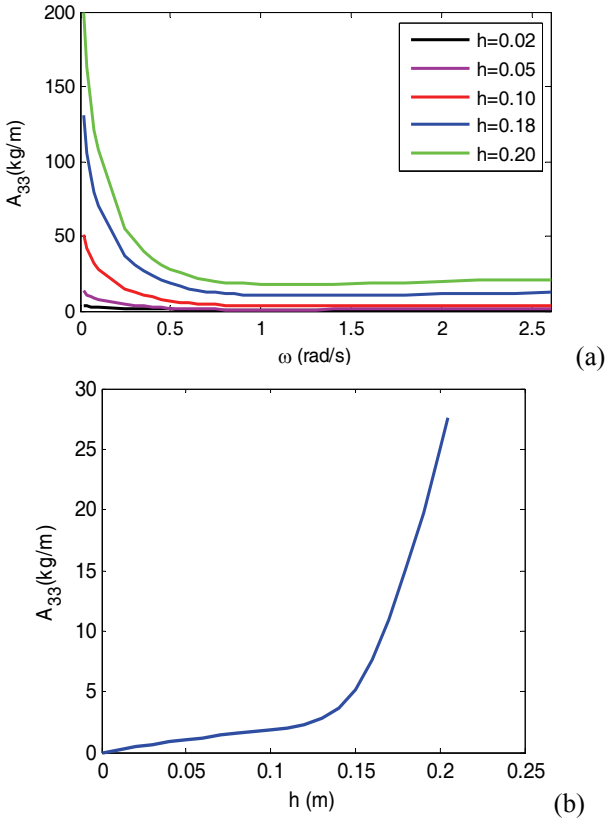

Figure 12. (a) Added mass for different submergence h. (b) High-frequency added mass as a function of submergence relative to calm water.

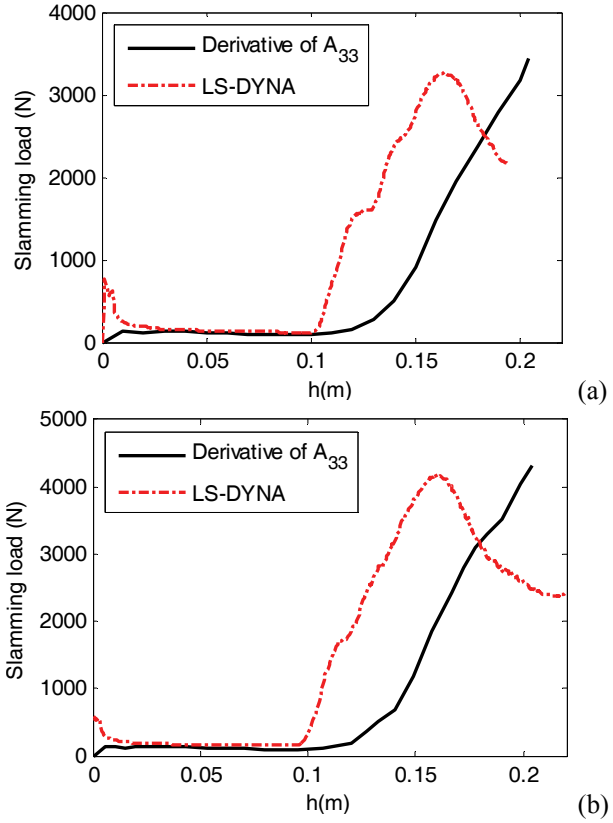

Figure 13. (a) Slamming load on the bow-flared section with constant entry velocity. (b) Slamming load on the bow-flared section with drop velocity.

5. CONCLUSIONS

The slam induced loads on a typical two-dimensional bow-flared section are evaluated by using the explicit finite element method based on multi-material formulation and an approximate method based on momentum theory. The numerical method gives reasonable predictions comparing to available experimental results.

The parametric study shows that the mesh density is the most important factor for the predictions of slam induced loads on the wetted surface of the bow-flared section. Combining the consideration of computational time, the model with mesh size of 0.008B, is more effective and economic. Another important parameter is the size of Region A. It is found that this size must be as big as the domain that water surface elevation spreads to and the penetration of the section during the entire water impact.

Fluid leakage through the structure, involving in the fluid-structure interaction, is a complicated problem and is difficult to prevent. In this work, the problem is prevented by using the donor cell advection algorithm which worked better than the penalty factor suggested in LS-DYNA Keyword User's Manual(2007). Simulated pressure distributions and pressure contours show that the maximum pressure is small and located at the keel of the bow-flared section in the initial stage of the water entry, while it moves to the region near the spray root of the water jet in the middle stage. After flow separation, the peak value moves downwards to the keel of the section. Though this method is applicable to this problem, high computational time is required.

For the approximation method, the slamming forces are calculated for two cases by considering the rate of change of the added mass. The peak forces are properly estimated, and they are slightly higher than the numerical ones. Without considering the effects of the water pile-up and the actual relative velocity, the time history of slamming force is not estimated accurately. One advantage of this method is the low computational efforts.

6. ACKNOWLEDGEMENTS

The work has been performed in the scope of the project EXTREME SEAS – Design for Ship Safety in Extreme Seas, (www.mar.ist.utl.pt/extremeseas), which has been partially financed by the EU under contract SCP8-GA-2009-234175. The added masses used in section 4.4 were calculated with the code developed by Suresh Rajendran, where the method of Ramos and Guedes Soares (1997) is implemented.

7. REFERENCES

1. AARSNES, J.V. (1996). Drop test with ship sections-effect of roll angle. *Report 603834.00.01. Norwegian Marine Technology Research Institute*, Trondheim.
2. ALEXANDRU, I., BRIZZOLARA, S., VIVIANI, M., COUTY, N., DONNER, R., HERMUNDSTAD, O., KUKKANEN, T., MALENICA, S., TERMAREL, P. (2007). Comparison of experimental and numerical impact loads on ship-like sections. *Advancements in Marine Structures, Guedes Soares, C, and Das, P.K., (Eds), Taylor and Francis*, UK, pp: 339-349.
3. AQUELET, N., SOULI, M., OLOVSSON, L. (2006). Euler–Lagrange coupling with damping effects: Application to slamming problems. *Comput. Methods Appl. Mech. Engrg., Volume 195*, pp: 110–132.
4. BELYTSCHKO, T. (1977). Methods and programs for analysis of fluid-structure system. *Nucl. Eng. Des., Volume 42*.
5. FALTINSEN, O.M., KVALSVOLD, J. AARSNES, J.V. (1997). Wave impact on a horizontal elastic plate, *J Mar Sci Technol., Volume 2*, pp: 87-100.
6. FONSECA, N., ANTUNES, E., GUEDES SOARES, C. (2006). Whipping response of vessels with large amplitude motions. *Proceedings of OMAE2006, 25th International Conference on Offshore Mechanics and Arctic*

Engineering, June 4-9, Hamburg, Germany. pp. 433-442.

7. GUEDES SOARES, C. (1989). Transient Response of Ship Hulls to Wave Impact. *International Shipbuilding Progress, Volume 36(406)*, pp: 137-156.
8. KAPSENBERG, G.K., THORNHILL, E.T. (2010). A practical approach to ship slamming in waves. *28th Symposium on Naval Hydrodynamics*, Pasadena, California, 12-17 Sep.
9. LUO, H.B., WANG S., GUEDES SOARES C. (2011). Numerical prediction of slamming loads on rigid wedge for water entry problem by an explicit finite element method. *Advances in Marine Structures, Guedes Soares, C, and Fricke, W., (Eds), Taylor and Francis*, UK, pp: 41-47.
10. LS-DYNA Keyword User's Manual, Livermore Software Technology Corporation, Version 971, May 2007.
11. MEI, X.M., LI, Y.M., DICK, K.P. (1999). On the water impact of general two-dimensional sections. *Appl. Ocean Res., Volume 21*, pp: 1-15.
12. OCHI, M.K., MOTTER, L.E. (1973), Prediction of slamming characteristics and hull response for ship design, Transactions SNAME, Volume 81, pp: 144-190.
13. OKADA, S. SUMI, Y. (2000). On the water impact and elastic response of a flat plate at small impact angles, *J Mar Sci Technol., Volume 5*, pp: 31-39.
14. RAMOS, J., GUEDES SOARES, C. (1997). On the assessment of hydrodynamic coefficients of cylinders in heaving. *Ocean Engng. Vol.24, No.8*, pp. 743-763.
15. RAMOS, J., GUEDES SOARES, C. (1998). Vibratory response of ship hulls to wave impact loads. *International Shipbuilding Progress, Volume 45(441)*, pp: 71-87.
16. RAMOS, J.; INCECIK, A., and GUEDES SOARES, C. (2000). Experimental Study of Slam Induced Stresses in a Containership. *Mar. Struct., Volume 13(1)*, pp: 25-51.
17. STAVOVY, A.B., CHUANG, S.L. (1976), Analytical determination of slamming pressures for high speed vessels in waves, *Journal of Ship Research, Volume 20*, pp: 90-198.
18. STENIUS, I., ROSN, A., KUTTENKEULER, J. (2006). Explicit FE-modelling of fluid–structure interaction in hull–water impacts. *International Shipbuilding Progress, Volume 53*, pp: 103-121.
19. SUN, H., FALTINSEN, O.M. (2009). Water entry of a bow flare section with a roll angle. *J Mar Sci Technol., Volume 14*, pp: 69-79.
20. VON KARMAN, T. (1929). The impact on seaplane floats during landing. *National Advisory Committee for Aeronatics. Techinical note No. 321*, 309-313.
21. WAGNER, H. (1932). Uber Stoss- und Gleitvergange an der Oberflache von Flussigkeiten. *Zeitschrift fuer Angewandte Mathematik und Mechanik, Volume 12*, pp: 193–215.
22. WANG, S., LUO, H.B., GUEDES SOARES, C. (2011). Explicit FE simulation of slamming load on rigid wedge with various deadrise angles during water entry. *Maritime Technology and Engineering, Guedes Soares, C, et al. (Eds), Taylor and Francis*, UK.
23. WANG, S., GUEDES SOARES, C. 2012. Analysis of the Water Impact of Symmetric Wedges with a Multi-Material Eulerian Formulation, *International Journal of Maritime Engineering, Volume 154, Part A4*, pp 191-206.
24. WANG, S., GUEDES SOARES, C. 2013. Slam induced loads on bow-flared sections with various roll angles, *Ocean Engi-neering, Vol. 67*, pp 45-57.
25. WANG, S., GUEDES SOARES, C. 2014. Asymmetrical water impact of two-dimensional wedges with roll angle with multi-material Eulerian formulation, *International Journal of Maritime Engineering, Volume 156, Part A2*, pp 115-130.
26. YETTOU, E1-M., DESROCHERS A. and Y. CHAMPOUX. (2007). A new analytical model for pressure estimation of symmetrical water impact of a rigid wedge at variable velocities. *J. Fluids Struct., Volume 23*, pp: 501-522.
27. ZHAO, R., FALTINSEN, O.M. (1993). Water Entry of Two-Dimensional Bodies. *J Fluid Mech., Volume 246*, pp: 593-612.
28. ZHAO, R., FALTINSEN, O.M., AARSNES, J.V. (1996). Water entry of arbitrary two-dimensional sections with and without flow separation. *Proc. 21st Symposium on Naval Hydrodynamics*, pp 408-423.
29. ZIENKIEWICZ, O.C., BETTESS, P. (1978). Fluid-structure dynamic interaction and wave forces. An introduction to numerical treatment. *Int. J. Numer. Meth. Eng., Volume 13(1)*, pp; 1-16.

